Acta Biomaterialia xxx (xxxx) xxx

Contents lists available at ScienceDirect

Acta Biomaterialia

journal homepage: www.elsevier.com/locate/actbio

Full length article

Unravelling the structural variation of lizard osteoderms

Arsalan Marghoub[a], Catherine J.A. Williams[b,c], João Vasco Leite[d], Alexander C. Kirby[e], Loïc Kéver[f], Laura B. Porro[e], Paul M. Barrett[d,g], Sergio Bertazzo[h], Arkhat Abzhanov[i], Matthew Vickaryous[c], Anthony Herrel[f], Susan E. Evans[e], Mehran Moazen[a,*]

[a] Department of Mechanical Engineering, University College London, London WC1E 7JE, UK
[b] Department of Biology, Aarhus University, Ny Munkegade 114-116, DK-8000 Aarhus C, Denmark
[c] Department of Biomedical Sciences, University of Guelph, 50 Stone Road East, Guelph, ON, N1G 2W1, Canada
[d] Department of Earth Sciences, Natural History Museum, Cromwell Road, London, SW7 5BD, UK
[e] Centre for Integrative Anatomy, Department of Cell and Developmental Biology, University College London, London, WC1E 6BT, UK
[f] UMR 7179 MECADEV C.N.R.S/M.N.H.N., Département Adaptations du Vivant, Bâtiment d'Anatomie Comparée, 55 rue Buffon, 75005, Paris, France
[g] Department of Earth Sciences, University College London, London, WC1E 6BT, UK
[h] Department of Medical Physics and Biomedical Engineering, University College London, London, WC1E 6BT, UK
[i] Department of Life Sciences, Faculty of Natural Sciences, Imperial College London, Silkwood18 Park Campus, Berkshire, SL5 7PY, UK

ARTICLE INFO

Article history:
Received 4 January 2022
Revised 12 April 2022
Accepted 3 May 2022
Available online xxx

Keywords:
Biomechanics
Skull
Cranial bone
Material characterisation
Biomaterials

ABSTRACT

Vertebrate skin is a remarkable organ that supports and protects the body. It consists of two layers, the epidermis and the underlying dermis. In some tetrapods, the dermis includes mineralised organs known as osteoderms (OD). Lizards, with over 7,000 species, show the greatest diversity in OD morphology and distribution, yet we barely understand what drives this diversity. This multiscale analysis of five species of lizards, whose lineages diverged ~100–150 million years ago, compared the micro- and macrostructure, material properties, and bending rigidity of their ODs, and examined the underlying bones of the skull roof and jaw (including teeth when possible). Unsurprisingly, OD shape, taken alone, impacts bending rigidity, with the ODs of *Corucia zebrata* being most flexible and those of *Timon lepidus* being most rigid. Macroscopic variation is also reflected in microstructural diversity, with differences in tissue composition and arrangement. However, the properties of the core bony tissues, in both ODs and cranial bones, were found to be similar across taxa, although the hard, capping tissue on the ODs of *Heloderma* and *Pseudopus* had material properties similar to those of tooth enamel. The results offer evidence on the functional adaptations of cranial ODs, but questions remain regarding the factors driving their diversity.

Statement of Significance

Understanding nature has always been a significant source of inspiration for various areas of the physical and biological sciences. Here we unravelled a novel biomineralization, i.e. calcified tissue, OD, forming within the skin of lizards which show significant diversity across the group. A range of techniques were used to provide an insight into these exceptionally diverse natural structures, in an integrated, whole system fashion. Our results offer some suggestions into the functional and biomechanical adaptations of OD and their hierarchical structure. This knowledge can provide a potential source of inspiration for biomimetic and bioinspired designs, applicable to the manufacturing of light-weight, damage-tolerant and multifunctional materials for areas such as tissue engineering.

1. Introduction

Vertebrate skin is a remarkable organ that helps to support and protect the body, acting as an interface between the organism and its environment. The skin consists of two layers – the epidermis (derived from ectoderm) and the underlying dermis (originating from mesoderm and neural crest), separated by a fibrous basement membrane [1]. The dermis includes cutaneous nerves, blood vessels, and variable amounts of glandular and fatty tissue. It may also include mineralised organs such as the elasmoid scales of teleost fish or the osteoderms (OD) that develop in many tetrapods. Unlike

* Corresponding author.
E-mail address: m.moazen@ucl.ac.uk (M. Moazen).

https://doi.org/10.1016/j.actbio.2022.05.004

epidermal scales, which are composed primarily of keratin proteins, mineralised skin organs include varying amounts of organic (e.g. collagen) and inorganic (hydroxyapatite) material. Mineralised organs within the skin date back to the Ordovician (~500 Ma), and demonstrate a diversity of different tissue types including bone, dentine, and enamel-like layers [2]. Among tetrapods, the majority of mineralised skin organs are composed primarily of bone, and hence are referred to as osteoderms (= *bone skin*). Less common are the dermal scales of gymnophionan amphibians (caecilians) and the lamina calcarea of some frogs and toads. Whereas gymnophionan dermal scales closely resemble the elasmoid scales of teleost fish, the lamina calcarea – an unusual calcified layer found within the dermis of tadpoles and adults – appears to lack any obvious comparisons with other vertebrate hard tissues [3].

ODs have been reported from representative members of most major extant tetrapod lineages including amphibians (various frog species), mammals (such as the armadillo), and reptiles (turtles, crocodilians, and many lizards) [4–7]. Lizards, with over 7,000 species, show the greatest diversity in OD morphology and distribution, yet our understanding of their structure, development, and function remains limited [8]. In lizards, ODs may be completely absent, present in restricted areas, or found all over the body in varied arrangements: as non-overlapping mineralised clusters; as a continuous covering of overlapping plates; or as spicular mineralisations that thicken with age and show a variety of structural designs [3,9]. What drives this extraordinary diversity is still an unsolved puzzle [8].

Several authors have carried out detailed histological analysis of lizard ODs to explore their developmental origin and biological constituents [6, 10–13]. Nevertheless, only a few studies have characterised their overall morphology [9,14,15]. Even fewer studies have characterised their mechanical properties (e.g. elastic modulus) or biomechanics [16–18] despite a significant body of literature for other taxa, such as alligators, armadillos, and various fishes [19–22]. A better understanding of these structures in lizards has the potential to lead to the development of bioinspired and biomimetic structures and devices [15, 23–29].

Here, we investigated ODs from five species of lizards that live in different habitats and whose lineages (Scincoidea, Lacertoidea, Anguimorpha) diverged from one another ~100–150 million years ago (Fig. 1): *Corucia zebrata*, a large (total length [TL] up to 800 mm), herbivorous (leaves, fruit) scincid that lives in the tree canopy and rarely comes to the ground [30,31]; *Timon lepidus*, a large (TL up to 600 mm), mainly ground-dwelling lacertid that feeds on large insects, beetles, spiders, snails, and some fruit [32]; *Heloderma suspectum*, a large (TL up to 600 mm), ground-dwelling venomous helodermatid anguimorph with a varied diet including eggs, small mammals, birds, and snakes [33]; *Pseudopus apodus*, a large (TL up to 1200 mm), limbless anguid that feeds on a range of insects, gastropods, and small vertebrate prey [34], and moves both on and below ground [35,36]; and the varanid anguimorph *Varanus komodoensis*, the largest extant lizard (TL ~3000 mm), which is an active venomous carnivore that feeds mainly on relatively large mammals [37–39]. As *V. komodoensis* material was unavailable for some analyses, in these cases we substituted material from its African relative, *V. niloticus* (TL 1200–2200 mm).

The macro- and microstructure of the ODs were described for each species using microCT and histological analysis, respectively. The mechanical properties of each OD and its component tissues were characterised using nano-indentation. To compare the mechanical properties of ODs with other mineralised tissues from the same species, we also measured the mechanical properties of components of the frontal bone, dentary, and, where possible, teeth, all taken from fresh frozen specimens. However, as skull material of *V. komodoensis* was not available for sampling, we substituted bone samples from a skull of *V. niloticus* that was of comparable size to those of the other lizards studied. Finally, given the observed diversity in the morphology and mechanical properties of the ODs, we used finite element analysis to assess the bending rigidity of the ODs along both the antero-posterior and transverse axes, focusing on the impact of shape and size variability, rather than any differences in their component tissues.

2. Materials and methods

2.1. Sample collection

Adult lizards were obtained from the Evans Lab (UCL). These specimens were donated by the Pathology Department, Zoological Society of London, and died of natural causes over a prolonged period; as such the precise date and time of death is unknown and varied between animals. The skull, mandible, and skin samples for single OD extraction were taken from animals that had been frozen (ca. -20° C) upon receipt. Note that: (1) although the varanid skin sample was taken from *V. komodoensis*, the skull and dentary samples were from *V. niloticus* as skull bone samples from *V. komodoensis* were not available for destructive sampling. These samples were then used for morphological, histological, finite element analysis, and material characterisation. *V. niloticus* has not been recorded as having OD in its skin [9] and we found no trace of them in our CT scans and dissections; and (2) one OD from either the head or the neck region (see Fig. 1) of one animal per species was used in each of the following characterisation methods.

The low number of samples per test (mainly due to specimen availability) is a limitation. However, we cross-checked our findings: (1) a single OD from the same anatomical region of the same *H. suspectum* was indented where the same pattern was observed as presented here [see 18]; (2) ODs from two other *H. suspectum,* from the head and from the same anatomical region as this study, were sectioned for visualisation purposes and the same patterns were observed; (3) ODs from two other *C. zebrata,* from the head, were sectioned for visualisation purposes and the same patterns were observed. Hence, we have confidence in the data presented herein, especially the relative differences reported, despite the small sample number. Note that limited sampling is also in line with the principals of animal Replacement, Reduction, and Refinement (3Rs).

2.2. Morphological analysis

With the exception of *V. komodoensis*, the whole head, as well as single OD (one sample from each specimen), were imaged using the micro-computed tomography (microCT) Nikon XT H 225 ST scanner (Nikon Metrology Ltd., UK) at University College London. MicroCT images were imported into the image processing software Avizo (Thermo Fisher Scientific, Mass, USA) and were manually segmented. 3D reconstructions of the ODs were used to carry out basic morphological measurements (length, width, height, volume, surface area) as shown in Fig. 2.

2.3. Histological analysis

Dissected skin samples were defrosted at room temperature and fixed in 20x volume of 10% neutral buffered formalin for at least 24 h, then placed in decalcification solution (1.9% glutaraldehyde, 0.15 M EDTA, in 0.06 M sodium cacodylate buffer, adjusted to 7.4 pH) at 4°C, changing to a fresh solution every 7 days, for 4 weeks. Further decalcification was performed prior to embedding using a Sakura TDE^{TM}30 Electrolysis Decalcifier System (Item Code 1427) and Sakura TDE^{TM}30 Decalcifier Solution (Item Code

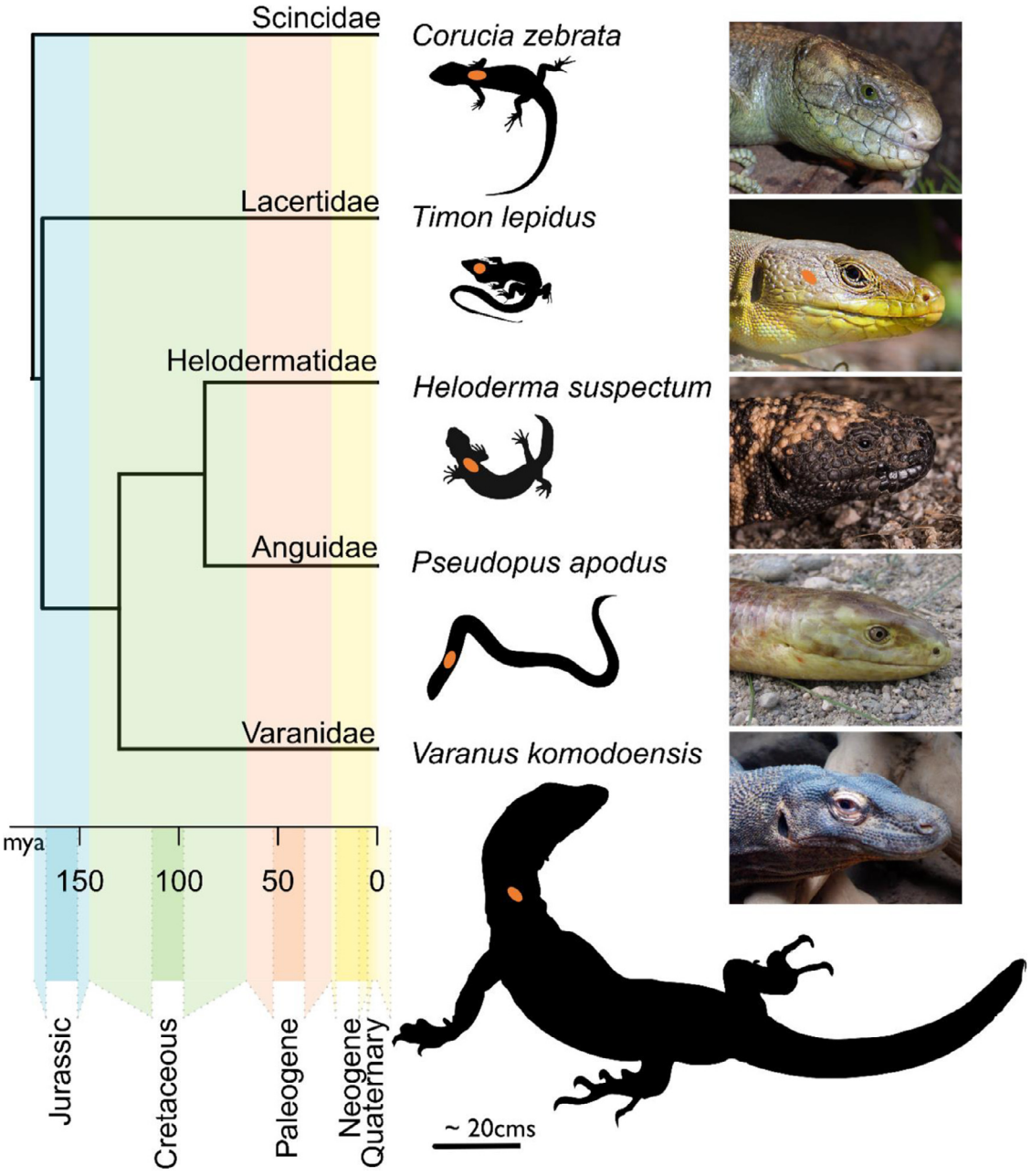

Fig. 1. A time-calibrated phylogeny of the species used in this study with approximately scaled silhouettes for representative adult whole body appearance with marked positions of single OD extractions (orange ovals – dorsal neck sampling for species where OD are present at that location, and marked as cranial OD for *Timon lepidus*). Photographs are showing external cranial appearance of the lizard species sampled. The phylogeny was created from data in Tonini et al. [59] using R studio and phytools (R Studio Team, 2015) [60]. Silhouettes are credited to the acknowledged artists under CC or Public Domain Dedication licenses, either via phylopic.org or by one of the authors (CW). Photographs are credited to the acknowledged photographers and used under CC license conditions from https://search.creativecommons.org/: The figure was assembled in Inkscape.

1428). Samples were embedded in paraffin wax and sectioned either coronally or parasagittally, at 5 μm thickness, with an HM Microm 355S automatic rotary microtome (Thermo Fisher Scientific). These sections were then stained with haematoxylin and eosin (H&E) [40], Masson's trichrome [41]. The slides were imaged using a Leica SCN400 scanner, and visualised and analysed in Apero Imagescape, and Qpath 0.2.3.

2.4. Material characterisation

Dissected ODs (one per species) and coronal sections of frontal and dentary bone (cut at the same point in each species, also one specimen per species) were embedded in cold cure epoxy resin (Buehler, Germany). After 24 h, the samples were cut and polished in the coronal plane. Polishing was performed using silicon carbide paper (320,600, 1200, and 2500 grit), and aluminium oxide slurries (0.3 and 0.05 μm particle size) on neoprene cloth (Buehler, Germany). The polishing protocol led to a final surface roughness of ~0.2 μm. Nanoindentation was then performed at room temperature using an Anton Paar system (UNHT^3, Anton Paar GmbH, Switzerland). A Berkovich diamond tip was employed as it has been widely used for indentation of hard calcified tissues [42–44]. Various regions were indented under displacement-control to a depth of 2.5 μm at 120 mN/min followed by 20 s hold [44,45]. A minimum spacing of 10 µm between the indents was ensured [42,44]. The elastic modulus was calculated using the

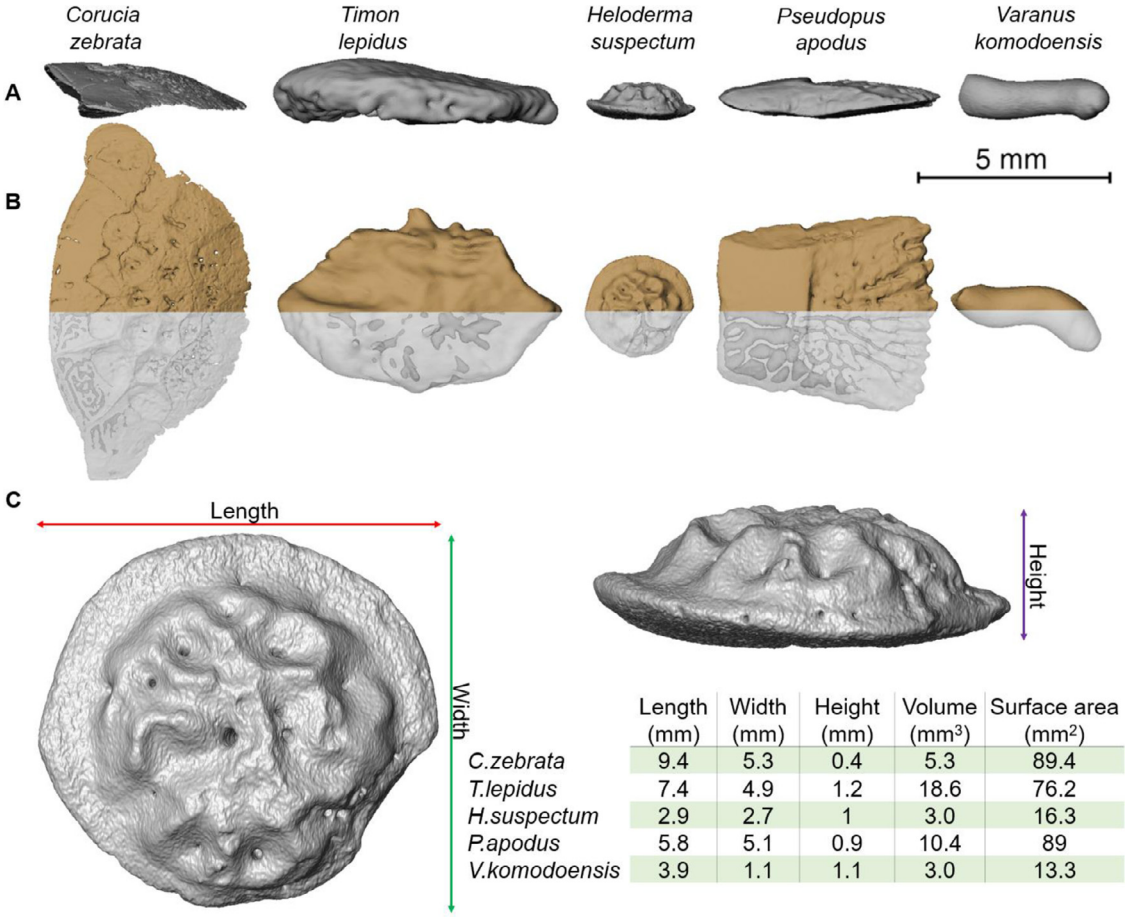

	Length (mm)	Width (mm)	Height (mm)	Volume (mm^3)	Surface area (mm^2)
C.zebrata	9.4	5.3	0.4	5.3	89.4
T.lepidus	7.4	4.9	1.2	18.6	76.2
H.suspectum	2.9	2.7	1	3.0	16.3
P.apodus	5.8	5.1	0.9	10.4	89
V.komodoensis	3.9	1.1	1.1	3.0	13.3

Fig. 2. Morphological variation in the ODs of five lizards. (A, B) show the lateral (A) and dorsal (B) views of a single OD. In (B) one half of each OD, uncoloured, has been rendered transparent to show any internal marrow cavities. (C) shows the various measurements undertaken and a summary of the quantified parameters on a single OD representative of the study species.

standard Oliver-Pharr method [46]. Here, the Poisson's ratio of the indented tissue and indenter tip were assumed to be 0.3 and 0.07, respectively, with the elastic moduli of the indenter tip being 1140 GPa (based on the manufacturer's data).

2.5. Finite element analysis

Three-dimensional models of individual OD were developed from microCT data. CT images were reconstructed in Avizo image processing software where a 3D surface model of each OD was transformed into a meshed solid geometry. The meshed geometries were imported into finite element software (ANSYS, PA, USA). The models were meshed using SOLID187 tetrahedral elements (10 node elements with quadratic displacement behaviours), that are well-suited for modelling irregular geometries. Mesh convergence was carried out, with the final models having approximately 1,000,000 elements for *C. zebrata*, *H. suspectum*, *P. apodus*, and *V. komodoensis*, and about 500,000 for *T. lepidus*. ODs were assigned isotropic material properties with an elastic modulus of 10 GPa and Poisson's ratio of 0.3. The exact values of the aforementioned properties were of less importance given that the relative comparison of mechanical performance between the OD morphologies was the main focus of the FE analysis. Three-point bending was modelled in two different planes (antero-posterior and transverse) as shown in Fig. 7. Here ODs were constrained at L/8 of the OD while a total load of 1 N (5×0.2 N) was applied at L/2 of the OD. Bending rigidity (EI) was then measured using the following equation:

$$EI = PL^3/48\omega_0$$

where P is the applied load, L is the length between two supports, and ω_0, is the total deflection at the point of loading. It is worth noting that our fundamental understanding of how ODs are loaded *in vivo* is limited; here we loaded the ODs in three-point bending as, given their wider arrangement within the skin, we considered that they are likely to be loaded in this mode *in vivo*. Nonetheless, the main focus of the analysis performed here was to use computational models to isolate morphological variations observed between the ODs and then investigate the impact of this parameter on OD bending rigidity.

3. Results

3.1. Morphological and histological analysis

Morphological analysis revealed considerable diversity in the shape, size, and distribution of ODs across the species investigated (Fig. 2). *T. lepidus* was the only species in which ODs were limited to the head, whereas the other four species had ODs over most of the head and body. Whereas the ODs of most species are singular elements, those of *C. zebrata* (as for most scincid lizards) are compound: each OD is composed of several smaller elements or osteodermites that are linked via fibrous joints. As shown in Fig. 2B,

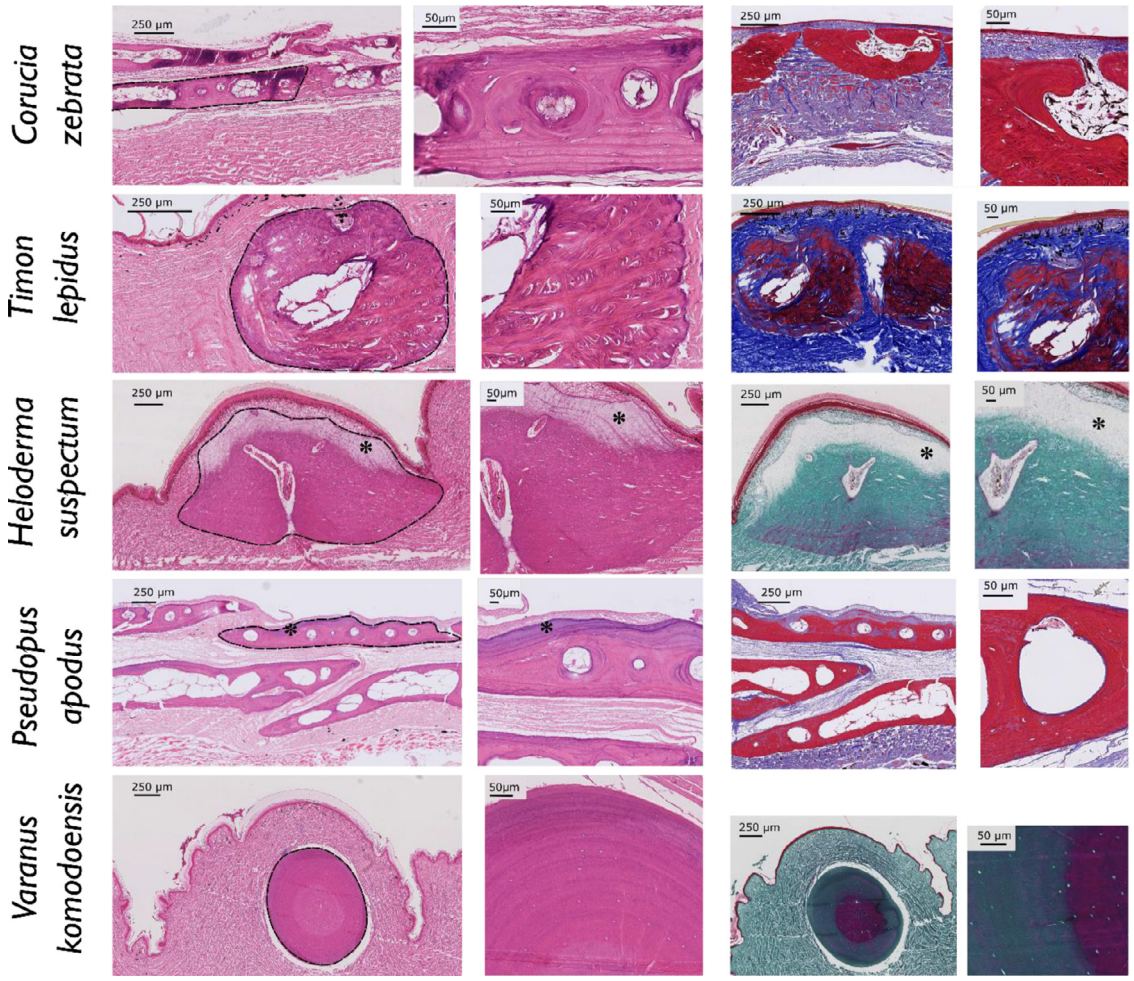

Fig. 3. Histological sections of ODs from the represented species with the epidermal surface dorsally (= uppermost). Left-side columns are stained using Haematoxalin and Eosin, and right-side columns using Massons' trichrome. Images show an overall view of the OD (scale bar 250 µm) and matching higher magnification panel (scale bar 50 µm). Sagittal views are shown for *C. zebrata*, and *P. apodus* to highlight the overlapping rows of OD and were also used for *H. suspectum* and *T. lepidus*; the OD of *V. komodoensis* is shown in transverse section to highlight the different fibre types. The OD is outlined by dashes in the H&E overview, and capping tissues are highlighted with '*' in *H. suspectum* and *P. apodus* sections.

ODs demonstrate species-specific variability in size, shape, and arrangement. Whereas *C. zebrata* ODs are broadly plate-like and overlapping, those of *T. lepidus* more closely resemble juxtaposed polygons, creating a mosaic-like arrangement. ODs in *H. suspectum* are also non-overlapping, but they are notably smaller than those of *T. lepidus*, with a roughly circular or hexagonal shape in dorsal profile. The ODs of *P. apodus* are trapezoidal and overlapping, whereas those of *V. komodoensis* resemble small cylinders, a shape referred to as vermiform. In addition to shape, ODs also differ in the presence and arrangement of internal cavities (Fig. 2B).

The histological analyses revealed unexpected microstructural diversity, including variation in tissue composition and arrangement (Fig. 3). As expected, ODs from all species were dominated by bone. However, the fibrillar organisation of the mineralised matrix, along with the inconsistent presence of a denser capping tissue (discussed below), varied between species.

C. zebrata ODs consist of a series of plates (osteodermites), each of which is composed of a combination of woven-fibred, Sharpey-fibred, and lamellar bone. Woven-fibred and Sharpey-fibred bone was generally associated with the periphery of each osteodermite, where adjacent elements were anchored to each other as well as to the surrounding dermis. Lamellar bone was characteristic of more central regions of each osteodermite surrounding the large marrow cavities and secondary osteons. Compared to the ODs of *C. zebrata*, those of *T. lepidus* demonstrated a less ordered microstructure, with numerous large penetrating Sharpey's fibres passing deep into each element, surrounded by a woven-fibred matrix. In section, *H. suspectum* ODs reveal a thick base of bone overlain by a distinct vitreous capping layer. The bony base is dominated by Sharpey-fibred bone, anchoring each element in the dermis. Neurovascular canals that invade the ODs are lined with a thin layer of lamellar bone. Capping the bony base is a thick layer of collagen-poor tissue with scarce cells, known as osteodermine [10,13,18]. ODs from *P. apodus* also develop a collagen-poor capping tissue, although it remains unclear if this tissue is homologous with the osteodermine characteristic of *H. suspectum* (highlighted in Figs. 3 & 4 with '*' in the *H. suspectum* and *P. apodus* sections). Deep to the capping tissue, *P. apodus* ODs are composed of Sharpey-fibred and lamellar bone. *V. komodoensis* ODs lack a capping tissue. In section, they have a concentric organisation with a core of woven-fibred bone, surrounded by parallel-fibred and lamellar bone.

At the scale of the whole sheet of OD level, cross-sectional analysis at the level of the frontal bone (Fig. 5) highlighted that ODs of *C. zebrata* are loosely connected to the underlying bone in this region. However, ODs of *H. suspectum* and *P. apodus* are fully fused to the frontal bone, although the degree of fusion increases with age in *Heloderma* (they can be detached from the skull with ease

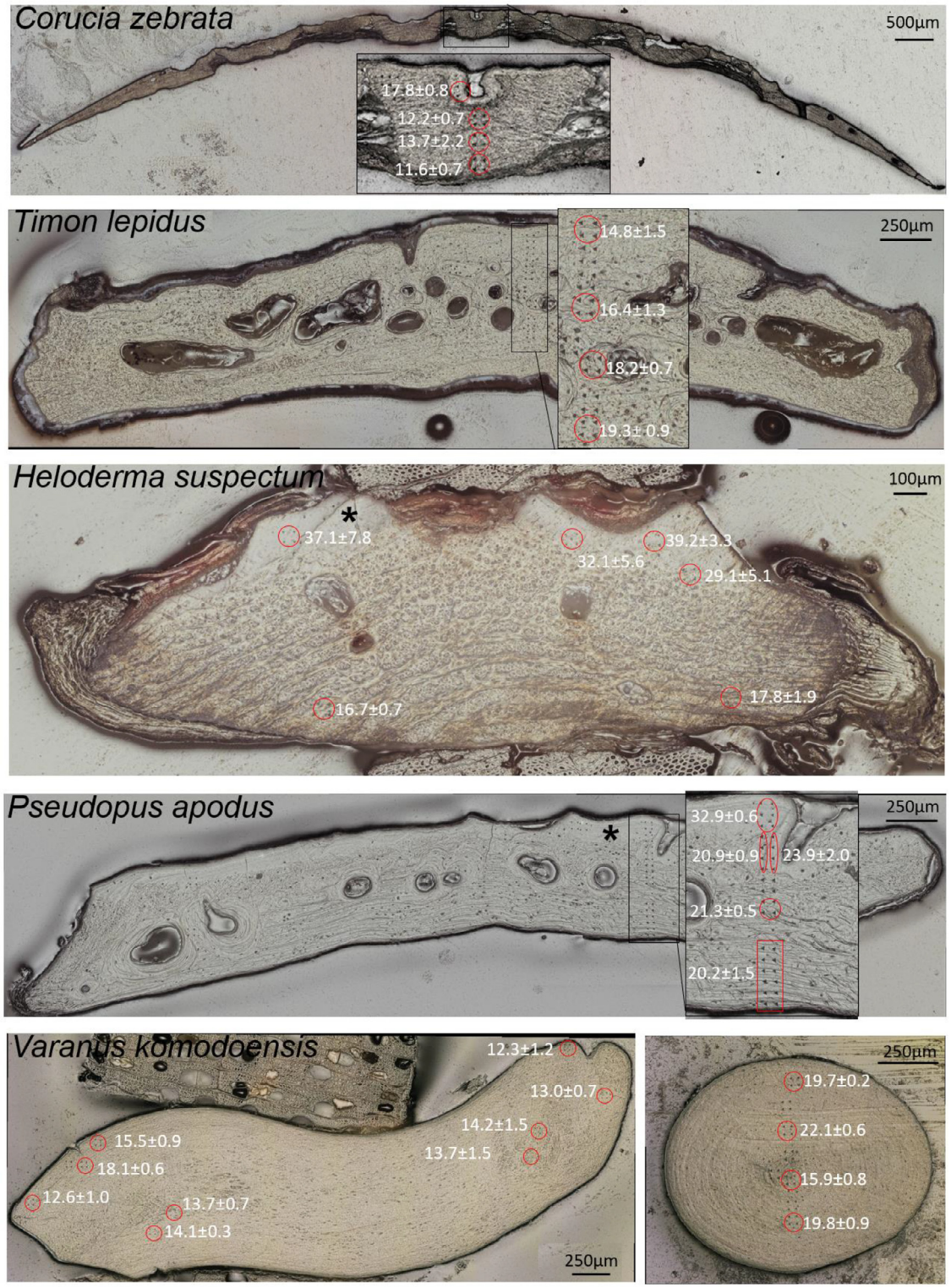

Fig. 4. Cross-section of ODs highlighting the mechanical properties of different regions of ODs in different species. Areas of nanoindentation are shown (black triangles) and were used to provide a mean ± standard deviation for each circled area of the section.

in young animals – personal observation). *T. lepidus* ODs are in the temporal region and across the supraorbital region. Their attachment to the parietal and frontal was not captured in the present study. However, our unpublished data show that there appears to be a thin layer of soft tissue present at the interface between ODs and skull roofing bones.

3.2. Material characterisation

Examination of the mechanical properties of *H. suspectum* and *P. apodus* ODs revealed that their mineralised capping tissue (highlighted in Fig. 4 with '*' in the *H. suspectum* and *P. apodus* sections) had similar mechanical properties that were very different

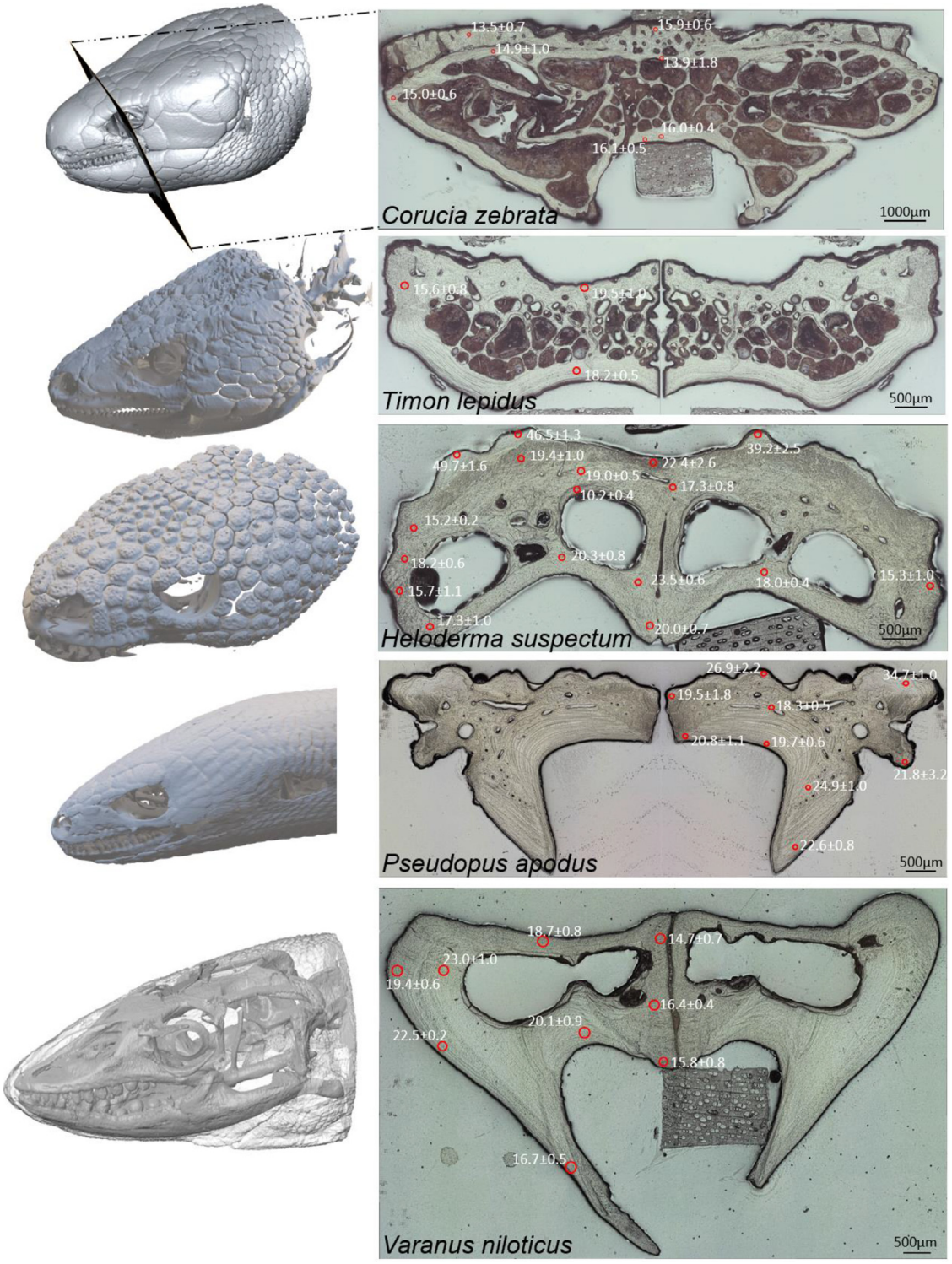

Fig. 5. Frontal sections of the skull in the five study species highlighting the mechanical properties of different regions of the section. Note: (1) *T. lepidus* and *P. apodus* sections were originally made for half of the skull and were virtually reconstructed to illustrate a complete section whereas the other sections are natural transverse sections of the entire frontal bone. (2) Areas of nanoindentation are shown (black triangles) and were used to provide a mean ± standard deviation for each circled area of the section.

from those of the other mineralised tissues in the skull, jaw, or ODs. The capping tissue displayed a higher elastic modulus and was much more similar to tooth enamel (Figs. 5 & 6). The inherent mechanical properties of the remaining regions of the ODs (i.e., except the capping tissue), despite some regional variability, were similar to those of the frontal and dentary bones from the same species (Table 1).

An unexpected finding was the distinct difference in the microstructure of the frontal and dentary bones between the species examined (Figs. 5 & 6). Transverse sections of the frontals of

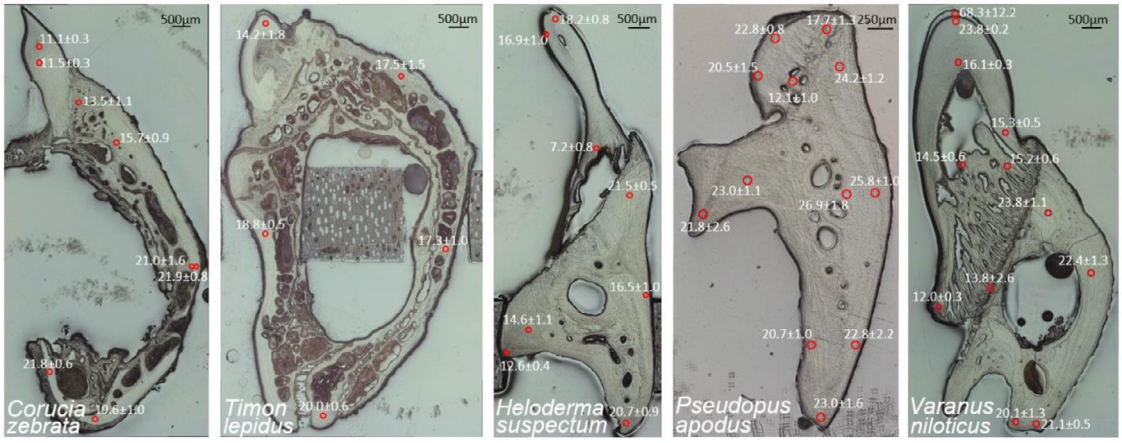

Fig. 6. A section of the dentary in the five study species highlighting the mechanical properties of different regions of the section. Areas of nanoindentation are shown (black triangles) and were used to provide a mean ± standard deviation for each circled area of the section.

Table 1
A summary of the quantified elastic modulus (of all indentations carried out) of different regions of the ODs, frontal bone, and dentary bone. Data are shown as ranges and in GPa.

Genus	Osteoderm		Frontal	Mandible		
	Bone	Capping tissue	Bone	Bone	Tooth Dentin	Enamel
C. zebrata	20.6 - 20.4	NA	10.7 – 20.7	12.8 - 24.3	6.8 - 13.6	NR
T. lepidus	10.5 - 21.7	NA	14.5 – 23.8	16.0 - 20.8	11.2 - 20.0	NR
H. suspectum	12.4 - 21.9	27.1 – 50.8*	15.0 – 24.4	12.3 - 22.3	15.1 - 18.6	22.4 - 39.9
P. apodus	15.7 - 23.4	19.7 – 35.9*	13.9 – 26.1	16.8 - 27.1	10.6 - 21.7	NR
V. komodoensis/niloticus^	14.8 - 23.2	NA	10.8 – 26.0	16.7 - 25.8	13.7 - 24.0	55.3 - 82.9**

* Recorded on the OD attached to the skull
** Recorded on the single tooth indentation
NA capping tissue was not present in these species
NR data for enamel of these species were not recorded
^ OD data are from *V. komodoensis*, while frontal and mandible data are from *V. niloticus*

C. zebrata and *T. lepidus* display a sandwich-like structure with compact dorsal and ventral layers separated by cancellous trabecular bone. A similar sandwich-like arrangement is present in *H. suspectum* and *V. niloticus* with central cavities but without the trabeculae. Interestingly, the frontal of *P. apodus* is strikingly different, with a relatively homogenous arrangement of compact bone throughout. Similarly, the dentaries of both *C. zebrata* and *T. lepidus* contain a significant number of cavities, compared to the compact bone of *H. suspectum*, *P. apodus*, and *V. niloticus*. The latter species also showed clearly folded plicidentine connecting the teeth to the jaw (Fig. 6).

3.3. Finite element analysis

Given the morphological and biomechanical differences between the ODs of the species studied, finite element analysis was carried out (Fig. 7) to assess the impact of morphological variation on the bending rigidity of individual ODs, using a three-point bending test. For this analysis we focussed solely on overall shape, and differences in bone microstructure or material properties were not considered (although they would, of course, be expected to be significant). As expected, the thin plate-like OD of *C. zebrata* had the lowest bending rigidity but, less predictably, that of a *T. lepidus* OD had the highest. Whereas the ODs of *T. lepidus* and *P. apodus* were of relatively similar size, those of *P. apodus* had an almost 60% lower bending rigidity. This could be explained by the fact that ODs of *P. apodus* are of lower height (thickness) and volume compared to *T. lepidus* ODs, and also because the harder capping tissue [47] was not modelled in this analysis. *H. suspectum* ODs showed a very similar bending rigidity across both axes (but the absence of the hypermineralised capping tissue in this test will have weakened the OD significantly [18]), whereas those of *V. komodoensis*, as expected from their cylindrical structure, showed the greatest difference in terms of the bending rigidity between the longitudinal and transverse axes. For the other three species, bending rigidity was relatively similar across both axes (Fig. 7C). It must be noted that bending rigidity is associated with strain distribution in the ODs. This is highlighted in Fig. 7, which illustrates that ODs with lower bending rigidity show higher levels of von Mises strain.

4. Discussion

This work provides insights into the remarkable diversity of lizard ODs and raises interesting questions about the factors driving these differences through their evolutionary history. The selective pressures driving the morphological diversity of lizard ODs remains largely unknown. Although OD probably affect the overall strength and mechanical properties of the skin [47,48], their presence, distribution, and diversity are likely to result from a combination of natural selection and developmental constraints. Similarly, the arrangement of internal cavities within the ODs probably reflects differences in vascularity and the development of marrow [8,13], and it may play a role in thermal regulation of the body.

The variation observed in frontal bone microstructure in the species studied is interesting and unpredicted. One potential explanation for the differences in frontal architecture between species might be a difference in feeding strategy or head use, and therefore in the degree and pattern of strain distributions across the skull [49–52]. From a biomechanical viewpoint, a thin solid frontal has lower bending rigidity than a thicker hollow frontal and is also

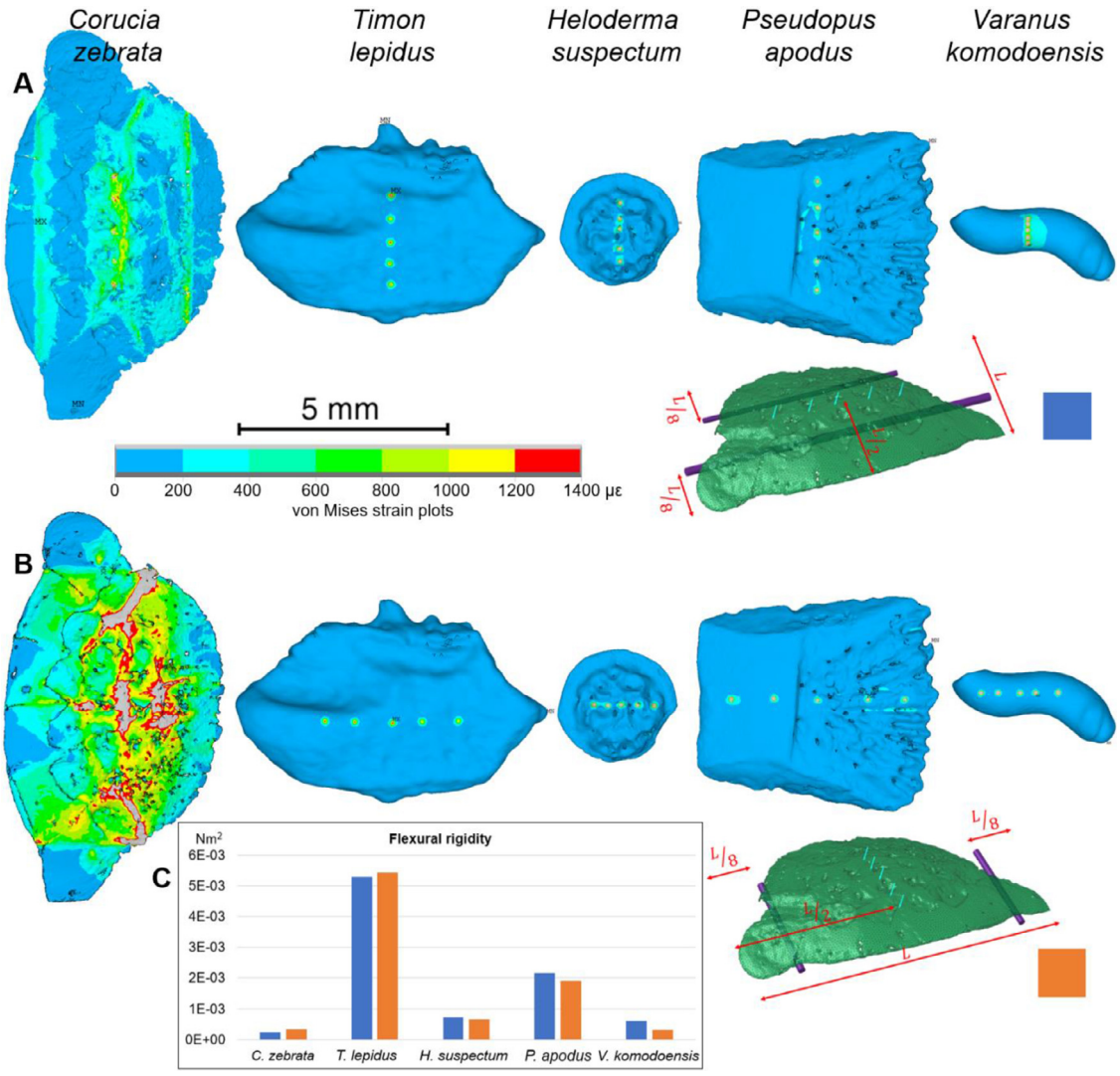

Fig. 7. Characterising the bending rigidity of the ODs in two planes (A, B) shows the pattern of von Mises strain during three-point bending. (C) is a summary of the bending rigidity of the ODs. Note that all ODs were rendered with the same material properties so that the focus was on the effect of shape alone.

less optimised in terms of mass reduction [e.g. 48]. Nonetheless, it is interesting that the ODs overlying the frontal of adult *P. apodus* are fully fused to the underlying bone (by comparison with the soft tissue gap present between the OD and the frontal bone in *C. zebrata*). This feature could help: (1) to mitigate the potentially lower strength of the frontal in *P. apodus* compared to the other species in this study; and (2) to reduce the level of mechanical strain experienced by the frontal and other adjacent bones arising from biting [53], or fighting. A similar explanation has been proposed for the fusion of cranial sutures (in e.g. lizards) where fusion can at least locally reduce the level of strain on the adjacent bones [54,55]. This could be another example of a highly optimised structure within the musculoskeletal system [56–58]. These findings, despite their preliminary nature, suggest that bone microstructure – of both ODs and skull elements – deserves a more comprehensive analysis as there may be a potential correlation between bite force, diet, and ecology.

Computational models highlighted the crucial role of morphology on the bending rigidity of the individual ODs. As expected, the thin plate-like OD of *C. zebrata* had the lowest bending rigidity and the thick OD of *T. lepidus* had the highest bending rigidity. Aside from the bending rigidity of the single ODs, it must be noted that the local balance of flexibility, protection, and reinforcement of the adjacent structures could also be achieved by variation in OD density and arrangement across the whole OD sheet, irrespective of the overall size and morphology of individual ODs [49]. Loosely connected ODs increase the overall flexibility of the OD sheet or its underlying structure (perhaps reflecting locomotion) while maintaining a degree of protection, most likely against conspecifics.

This study represents a first step in assessing the structural and biomechanical diversity of lizard ODs. Given that we analysed only five species out of over 3000 OD-bearing lizard taxa, it would be premature to speculate on the evolutionary significance of our findings or to draw general conclusions on the roles of ODs across lizard diversity. Nonetheless, we consider that our findings raise interesting questions and provide a strong foundation for further work on the microstructure and material properties of both ODs and skull bones. In the longer term, this will facilitate the exploration of the possible correlations between the presence, shape, and density of ODs and, for example, bite force, sprint speed, body size, lifestyle, and predation. Equally, although these results offer some insights into the functional and biomechanical adaptations of ODs, the extent to which their diversity is driven by genetic variation and developmental factors remains largely unknown.

5. Conclusions

Lizard ODs show remarkable diversity, not only in their overall morphology but also in their hierarchical structure and material properties. Analysis of the craniofacial system of the species studied here indicates a possible link in some species between overall skull performance, the microstructures of the frontal and dentary bones, and OD functional design. This, in turn, provides a strong foundation for wider surveys of lizard ODs in future multiscale and whole system level analyses. Moreover, the morphological variation seen in the cranial and mandibular bones of the five genera studied suggests a more comprehensive survey of different skull regions may provide valuable additional information, both on skull structure and function in lizards and their relatives. Finally, this work provides further evidence for the diversity of lizard OD, which might offer potential sources of biomimetic and bioinspired designs applicable to the manufacturing of light-weight, damage-tolerant, and multifunctional materials.

Declaration of Competing Interest

The authors declare that they have no known competing financial interests or personal relationships that could have appeared to influence the work reported in this paper.

Acknowledgements

This work was supported by the Human Frontier Science Program (RGP0039/2019) and Natural Environment Research Council (NE/R000077/1) to PMB and LBP. We thank (1) the Pathology Department (Zoological Society of London) for cadaveric material of the lizards used in this study; (2) Engineering and Physical Sciences Research Council for funding the 3D microscope that was used in this study through (EP/T023651/1); (3) Yiannis Ventikos and Manish Tiwari for their continuous support of imaging suite that was set up and used for this work at UCL Mechanical Engineering.

Photographs in Fig. 1 are from "Wickelschwanz-Skink - *Corucia zebrata*" by andrea.janitzki and is licensed under CC BY-NC-SA 2.0. "*Timon lepidus*" by AlexandreRoux01 is licensed under CC BY-NC-SA 2.0. "Gila Monster, *Heloderma suspectum* Cope, 1869" by Misenus1 is licensed under CC BY-NC-SA 2.0. "*Pseudopus apodus*", by Morteza Johari is licensed marked with CC Public Domain Mark 1.0. "Komodo Dragon, *Varanus komodensis*" by PopPETography is licensed under CC BY 2.0.

Silhouettes in Fig 1: *Varanus komodoensis* Peter Travers under Public Domain Dedication 1.0 license. *Heloderma suspectum*, Nicolas Mongiardino Koch under Public Domain Dedication 1.0 license. *Corucia zebrata*, Catherine Williams using illustrations by Kailah Thorn & Ben King under Public Domain Dedication licenses and photographic reference by Lubomír Klátil. *Pseudopus apodus*, Catherine Williams using photo references by Ron Knight licensed under CC BY 2.0. *Timon lepidus*, Catherine Williams using photo references by Bernard Dupont under CC BY-SA 2.0.

References

[1] A. Nyström, L. Bruckner-Tuderman, Matrix molecules and skin biology, Semin. Cell. Dev. Biol. 89 (2019) 136–146.
[2] J.Y. Sire, P.C.J. Donoghue, M.K. Vickaryous, Origin and evolution of the integumentary skeleton of non-tetrapod vertebrates, J. Anat. 214 (2009) 409–440.
[3] M.K. Vickaryous, J.Y. Sire, The integumentary skeleton of tetrapods: origin, evolution, and development, J. Anat. 214 (2009) 441–464.
[4] G.S. Bever, C.J. Bell, J.A. Maisano, The ossified braincase and cephalic osteoderms of *Shinisaurus crocodilurus* (Squamata, Shinisauridae), Palaeont. Electr. 8 (2005) 1–36.
[5] J.I. Mead, B.W. Schubert, S.C. Wallace, S.L. Swift, Helodermatid lizard from the Mio-Pliocene oak-hickory forest of Tennessee, eastern USA, and a review of monstersaurian osteoderms, Acta Palaeont. Polonica. 57 (2012) 111–121.
[6] M.K. Vickaryous, G. Meldrum, A.P. Russell, Armored geckos: a histological investigation of osteoderm development in *Tarentola* (Phyllodactylidae) and *Gekko* (Gekkonidae) with comments on their regeneration and inferred function, J. Morphol. 276 (2015) 1345–1357.
[7] D.J. Paluh, A.H. Griffing, A.M. Bauer, Sheddable armour: identification of osteoderms in the integument of *Geckolepis maculata* (Gekkota), Afr. J. Herpetol. 66 (2017) 12–24.
[8] C. Williams, A. Kirby, A. Marghoub, L. Kever, S. Ostashevskaya-Gohstand, S. Bertazzo, M. Moazen, A. Abzhanov, A. Herrel, S.E. Evans, M. Vickaryous, A review of the osteoderms of lizards (Reptilia: Squamata), Biol. Rev. 97 (2022) 1–19.
[9] J.A. Maisano, T.J. Laduc, C.J. Bell, D. Barber, The cephalic osteoderms of *Varanus komodoensis* as revealed by high-resolution X-ray computed tomography, Anat. Rec. 302 (2019) 1675–1680.
[10] M.L. Moss, Comparative histology of dermal sclerifications in reptiles, Acta Anatomica 73 (1969) 510–533.
[11] V. Levrat-Calviac, L. Zylberberg, The structure of the osteoderms in the gekko: *Tarentola mauritanica*, Am. J. Anat. 176 (1986) 437–446.
[12] V. de Buffrénil, J.Y. Sire, J.C. Rage, The histological structure of glyptosaurine osteoderms (Squamata: Anguidae), and the problem of osteoderm development in squamates, J. Morphol. 271 (2010) 729–737.
[13] A. Kirby, M. Vickaryous, A. Boyde, A. Olivo, M. Moazen, S. Bertazzo, S. Evans, A comparative histological study of the osteoderms in the lizards *Heloderma suspectum* (Squamata: Helodermatidae) and *Varanus komodoensis* (Squamata: Varanidae), J. Anat. 236 (2020) 1035–1043.
[14] D. Costantini, M.L. Alonso, M. Moazen, E. Bruner, The relationship between cephalic scales and bones in lizards: a preliminary microtomographic survey on three lacertid species, Anat. Rec. 293 (2010) 183–194.
[15] C. Liang, A. Marghoub, L. Kever, S. Bertazzo, A. Abzhanov, M. Vickaryous, A. Herrel, S. Evans, M. Moazen, Lizard osteoderms – morphological characterisation, biomimetic design and manufacturing based on three species, Bioinspir. Biomim. 16 (2021) 066011.
[16] C. Broeckhoven, G. Diedericks, P.L.F.N. Mouton, What doesn't kill you might make you stronger: functional basis for variation in body armour, J. Anim. Ecol. 84 (2015) 1213–1221.
[17] C. Broeckhoven, C. De Kock, P.L.F.N. Mouton, Sexual dimorphism in osteoderm expression and the role of male intrasexual aggression, Biol J. Linn. Soc. 122 (2017) 329–339.
[18] A.C. Kirby, F. Iacoviello, Y. Javanmardi, E. Moeendarbary, M. Shabanli, E. Tsolaki, A.C. Sharp, M.J. Hayes, K. Keevend, J.H. Li, D.J. Brett, P.R. Shearing, A. Olivo, I.K. Herrmann, S.E. Evans, M. Moazen, S. Bertazzo, The multiscale hierarchical structure of *Heloderma suspectum* osteoderms and their mechanical properties, Acta Biomater. 107 (2020) 194–203.
[19] I.H. Chen, J.H. Kiang, V. Correa, M.I. Lopez, P-Y. Chen, J. McKittrick, M.A. Meyers, Armadillo armor: mechanical testing and micro-structural evaluation, J. Mech. Behav. Biomed. Mater. 4 (2011) 713–722.
[20] I.H. Chen, W. Yang, M.A. Meyers, Leatherback sea turtle shell: a tough and flexible biological design, Acta Biomater. 28 (2015) 2–12.
[21] C.Y. Sun, P.Y. Chen, Structural design and mechanical behavior of alligator (Alligator mississippiensis) osteoderms, Acta Biomater. 9 (2013) 9049–9064.
[22] D. Zhu, L. Szewciw, F. Vernerey, F. Barthelat, Puncture resistance of the scaled skin from striped bass: collective mechanisms and inspiration for new flexible armor designs, J. Mech. Behav. Biomed. Mater. 24 (2013) 30–40.
[23] W. Yang, I.H. Chen, B. Gludovatz, E.A. Zimmermann, R.O. Ritchie, M.A. Meyers, Natural flexible dermal armor, Adv. Mater. 25 (2013) 31–48.
[24] L. Wen, J.C. Weaver, G.V. Lauder, Biomimetic shark skin: design, fabrication and hydrodynamic function, J. Exp. Biol. 217 (2014) 1656–1666.
[25] R.K. Chintapalli, M. Mirkhalaf, A.K. Dastjerdi, F. Barthelat, Fabrication, testing and modeling of a new flexible armor inspired from natural fish scales and osteoderms, Bioinspir. Biomim. 9 (2014) 36005–36014.
[26] S.M. Chen, H.L. Gao, Y.B. Zhu, H.B. Yao, L.B. Mao, Q.Y. Song, J. Xia, Z. Pan, Z. He, H.A. Wu, S.H. Yu, Biomimetic twisted plywood structural materials, Natl. Sci. Rev. 5 (2018) 703–714.
[27] S.E. Naleway, M.M. Porter, J. McKittrick, M.A. Meyers, Structural design elements in biological materials: application to bioinspiration, Adv. Mater. 27 (2015) 5455–5476.
[28] N. San Ha, G. Lu, A review of recent research on bio-inspired structures and materials for energy absorption applications, Compos. B. Eng. 181 (2020) 107496.
[29] A. Ingrole, T.G. Aguirre, L. Fuller, S.W. Donahue, Bioinspired energy absorbing material designs using additive manufacutring, J. Mech. Behav. Biomed. Mater. 119 (2021) 104518.
[30] W.E. Cooper, Food chemical discriminations by an herbivorous lizard, *Corucia zebrata*, J. Exp. Zool. 286 (2000) 372–378.
[31] L.J. Harmon, Some observations of the natural history of the prehensile-tailed skink, *Corucia zebrata*, in the Solomon Islands, Herpetol. Rev. 33 (2002) 177.
[32] J.M. Thirion, P. Grillet, M. Cheylan, Composition et variation saisonnière du régime alimentaire du Lézard ocellé *Timon lepidus* sur l'Île d'Oléron (France) à partir des fèces, Revue d'Écologie 64 (2009) 239–250.
[33] K.B. Jones, Movement patterns and foraging ecology of Gila Monsters (*Heloderma suspectum* Cope) in Northwestern Arizona, Herpetologica 39 (1983) 247–253.
[34] C.E. Burt, Insect food of Kansas lizards with notes on feeding habits, J. Kans. Entomol 1 (1928) 50–68.
[35] V.H. Hutchinson, J.L. Larimer, Reflectivity of the integuments of some lizards from different habitats, Ecology 41 (1960) 199–209.

[36] S. Kamel, R.E.J. Gatten, Aerobic and anaerobic activity metabolism of limbless and fossorial reptiles, Physiol. Zool. 56 (1983) 419–429.
[37] W. Auffenberg, The Behavioral Ecology of the Komodo Monitor, University Presses of Florida, Gainesville, Florida, 1981.
[38] C.J. Clemente, G.G. Thompson, P.C. Withers, Evolutionary relationships of sprint speed in Australian varanid lizards, J. Zool. 278 (2009) 270–280.
[39] A. Ariefiandy, Purwandana D, G. Coulson, D.M. Forsyth, T.S. Jessop, Monitoring the ungulate prey of the Komodo dragon *Varanus komodoensis*: distance sampling or faecal counts? Wildlife Biol. 19 (2013) 126–137.
[40] J. Kiernan, R. Lillie, P. Pizzolato, et al., Haematoxylin Eosin (H&E) staining protocols online. Available at: www.protocolsonline.com [Accessed: 05 June 2019].
[41] E.N. Calvi, F.X. Nahas, M.V. Barbosa, J.A. Calil, S.S. Ihara, M.de.S. Silva, M.F. Franco, L.M. Ferreira, An experimental model for the study of collagen fibers in skeletal muscle, Acta Cir. Bras. 27 (2012) 681–686.
[42] E. Donnelly, S.P. Baker, A.L. Boskey, M.C. van der Meulen, Effects of surface roughness and maximum load on the mechanical properties of cancellous bone measured by nanoindentation, J. Biomed. Mater. Res. A 77 (2006) 426–435.
[43] P.K. Zysset, Indentation of bone tissue: a short review, Osteoporos Int 20 (2009) 1049–1055.
[44] M. Moazen, E. Peskett, C. Babbs, E. Pauws, M.J. Fagan, Mechanical properties of calvarial bones in a mouse model for craniosynostosis, PLoS ONE 10 (2015) e0125757.
[45] U. Wolfram, H-J. Wilke, P.K. Zysset, Rehydration of vertebral trabecular bone: influences on its anisotropy, its stiffness and the indentation work with a view to age, gender and vertebral level, Bone 46 (2010) 348–354.
[46] W.C. Oliver, G.M. Pharr, An improved technique for determining hardness and elastic modulus using load and displacement sensing indentation experiments, J. Mat. Res. 7 (1992) 1564–1583.
[47] P. Fratzl, O. Kolednik, F.D. Fischer, M.N. Dean, The mechanics of tessellations—bioinspired strategies for fracture resistance, Chem. Soc. Rev. 45 (2016) 252–267.
[48] M. Connors, T. Yang, A. Hosny, Z. Deng, F. Yazdandoost, H. Massaadi, D. Eernisse, R. Mirzaeifar, M.N. Dean, J.C. Weaver, C. Ortiz, L. Li, Bioinspired design of flexible armor based on chiton scales, Nat. Commun. 10 (2019) 5413.
[49] A. Herrel, V. Schaerlaeken, J.J. Meyers, K.A. Metzger, C.F. Ross, The evolution of cranial design and performance in squamates: consequences of skull-bone reduction on feeding behavior, Integr. Comp. Biol. 47 (2007) 107–117.
[50] M. Moazen, N. Curtis, P. O'Higgins, S.E. Evans, M.J. Fagan, Biomechanical assessment of evolutionary changes in the lepidosaurian skull, PNAS 106 (2009) 8273–8277.
[51] C.E. Terhune, A.D. Sylvester, J.E. Scott, M.J. Ravosa, Internal architecture of the mandibular condyle of rabbits is related to dietary resistance during growth, J. Exp. Biol. 223 (2020) jeb220988.
[52] H. Dutel, F. Gröning, A.C. Sharp, P.J. Watson, A. Herrel, C.F. Ross, M.E.H. Jones, S.E. Evans, M.J. Fagan, Comparative cranial biomechanics in two lizard species: impact of variation in cranial design, J. Exp. Biol. 224 (2021) jeb234831.
[53] J. Xue, A. Marghoub, S. Bertazzo, S.E. Evans, M. Moazen, Biomechanics of osteoderms in a lizard skull–a preliminary finite element study, J. Anat. B18 (2017).
[54] M. Moazen, N. Curtis, S.E. Evans, P. O'Higgins, M.J. Fagan, Combined finite element and multibody dynamics analysis of biting in a *Uromastyx hardwickii* lizard skull, J. Anat. 213 (2008) 499–508.
[55] M. Moazen, N. Curtis, P. O'Higgins, M.E.H. Jones, S.E. Evans, M.J. Fagan, Assessment of the role of sutures in a lizard skull- a computer modelling study, Proc. Roy. Soc. B 276 (2009) 39–46.
[56] D. Carter, M. van der Meulen, G. Beaupré, Mechanical factors in bone growth and development, Bone 18 (1996) 5–10.
[57] U. Witzel, H. Preuschoft, Finite-element model construction for the virtual synthesis of the skulls in vertebrates: case study of Diplodocus, Anat. Rec. 283 (2005) 391–401.
[58] R. Gößling, M. Herzog, U. Witzel, B. Bender, Compensation of bending moments as a nature-inspired design principle? in: In: Design 2014: proceedings of the 13th International Design Conference, Dubrovnik, Croatia, 2014 May 19-22.
[59] J.F.R. Tonini, K.H. Beard, R.B. Ferreira, W. Jetz, R.A. Pyron, Fully-sampled phylogenies of squamates reveal evolutionary patterns in threat status, Biol. Conserv. 204 (2016) 23–31.
[60] L.J. Revell, Phytools: an R package for phylogenetic comparative biology (and other things), Methods Ecol. Evol. 3 (2012) 217–223.